Research Article

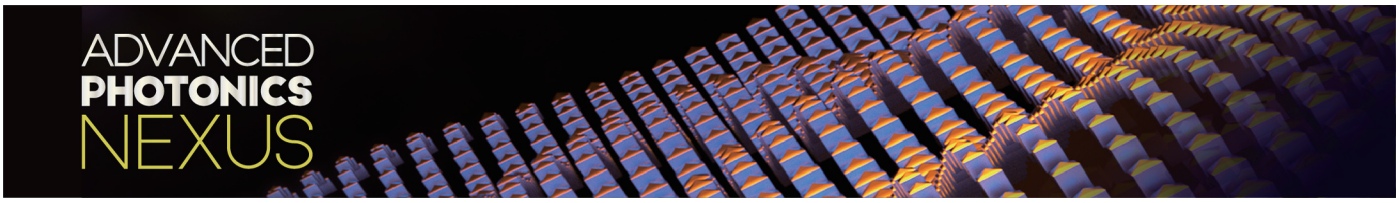


# High-repetition-rate seeded free-electron laser enhanced by self-modulation

**Hanxiang Yang**[a,b] **Jiawei Yan**[c] **and Haixiao Deng**[d,*]
[a]Chinese Academy of Sciences, Shanghai Institute of Applied Physics, Shanghai, China
[b]University of Chinese Academy of Sciences, Beijing, China
[c]European XFEL, Schenefeld, Germany
[d]Chinese Academy of Sciences, Shanghai Advanced Research Institute, Shanghai, China

**Abstract.** The spectroscopic methods for the ultrafast electronic and structural dynamics of materials require fully coherent extreme ultraviolet and soft X-ray radiation with high-average brightness. Seeded free-electron lasers (FELs) are ideal sources for delivering fully coherent soft X-ray pulses. However, due to state-of-the-art laser system limitations, it is challenging to meet the ultraviolet seed laser's requirements of sufficient energy modulation and high repetition rates simultaneously. The self-modulation scheme has been proposed and recently demonstrated in a seeded FEL to relax the seed laser requirements. Using numerical simulations, we show that the required seed laser intensity in the self-modulation is ~3 orders of magnitude lower than that in the standard high-gain harmonic generation (HGHG). The harmonic self-modulation can launch a single-stage HGHG FEL lasing at the 30th harmonic of the seed laser. Moreover, the proof-of-principle experimental results confirm that the harmonic self-modulation can still amplify the laser-induced energy modulation. These achievements reveal that the self-modulation can not only remarkably reduce the requirements of the seed laser but also improve the harmonic upconversion efficiency, which paves the way for realizing high-repetition-rate and fully coherent soft X-ray FELs.

Keywords: high repetition rate; free-electron laser; self-modulation; fully coherent; soft X-ray.

Received Dec. 4, 2022; revised manuscript received Feb. 23, 2023; accepted for publication Mar. 27, 2023; published online Apr. 18, 2023.



[DOI: 10.1117/1.APN.2.3.036004]

## 1 Introduction

High-gain free-electron lasers (FELs) can generate wavelength-tunable pulses of high brightness, opening a range of new research in various fields, including biology, chemistry, physics, and materials science.[1,2] However, most successful FEL-based experiments to date are based on the properties of single-shot pulses, such as the internal structure studies of materials.[3] In contrast, fully coherent FELs with high repetition rates are critical for some photon-hungry experiments, such as the fine time-resolved analysis of matter with spectroscopy and photon scattering.

Currently, most of the X-ray FEL (XFEL) facilities worldwide[4–8] are based on the mechanism of self-amplified spontaneous emission (SASE).[9,10] The SASE scheme can obtain high-brightness pulses with a sub-Ångstrom wavelength and a femtosecond duration. Because of the mode selection process, SASE pulses can become nearly transversely coherent. However, the longitudinal coherence of the SASE pulses is limited by the slippage of radiation within the FEL gain length. Self-seeding schemes[11,12] have been proposed to improve the longitudinal coherence, but at the cost of shot-to-shot intensity fluctuations.

Seeded FELs[13–17] that use a coherent external seed laser to trigger the initial amplification process of the XFEL are ideal for obtaining fully coherent FEL pulses with a small pulse energy fluctuation. In a typical configuration of seeded FELs, such as the high-gain harmonic generation (HGHG),[18] sinusoidal energy modulation is introduced by an external seed laser in a modulator through the laser–electron beam interaction. Then a magnetic chicane referred to as the dispersive section is used to convert the energy modulation into periodic density bunching

*Address all correspondence to Haixiao Deng, denghx@sari.ac.cn

comprising frequency components at high harmonics. Finally, the microbunched beams are sent through a relatively long undulator referred to as the radiator, in which the coherent radiation of the harmonic of interest is generated and further amplified through the FEL process. In addition, sophisticated phase-space manipulation techniques, such as the echo-enabled harmonic generation (EEHG)[15,16] and phase-merging enhanced harmonic generation,[17] have been developed to improve the frequency multiplication efficiency of the single stage. Both analytical calculations and experimental results demonstrate that seeded FELs can produce high-power soft X-ray radiation with a narrow bandwidth using an ultraviolet seed laser.[19–25]

In recent years, the high-repetition-rate operation of XFEL has been proposed to obtain pulses with high average brightness, which has enormous potential in a variety of scientific studies.[3,7,26–28] Based on superconducting accelerators, FLASH[29] and the European XFEL[7] can reach repetition rates of 1 and 4.5 MHz in a burst mode, respectively. Moreover, SHINE[27,28] and LCLS-II[26] are designed to achieve 1 MHz in a continuous-wave mode. A seeded FEL with a repetition rate of 1 MHz can meet the requirements of specific experiments, such as high-resolution spectroscopy techniques. However, it is currently impossible for state-of-the-art laser systems to obtain laser pulses with sufficient peak power for the energy modulation of the electron beam and at the same time have such a high repetition rate.

Different methods have been proposed to realize high-repetition-rate seeded FELs. Recently, the self-modulation of the electron beam has been experimentally demonstrated to be an effective method of reducing the requirement for an external seed laser.[30,31] Moreover, further studies have shown that the self-modulation method has a stability similar to HGHG and has the potential to achieve very high harmonics.[32,33] The utilization of an FEL oscillator as the seeding source for subsequent cascades has been proposed.[34–37] In addition, a resonator-like seed recirculation feedback system has been proposed to reuse the radiation in the modulator section to modulate the following electron bunches.[38–41] The use of a relatively longer modulator has been suggested to reduce the peak power requirements of the external seed laser.[32,42,43] More analysis of various methods to high-repetition-rate seeded FELs has been studied.[44] Compared with the seeded oscillator–amplifier scheme[40] and the modulator lengthening scheme,[43] the self-modulation scheme[30] does not require extra optical elements or a considerably long modulator. The self-modulation scheme can be easily applied to all existing seeded FEL facilities with minimal hardware addition, especially in synergy with EEHG setups.

In this work, we first systematically analyze the crucial parameters in the self-modulation scheme to provide design and optimization directions for its further application in seeded FELs, such as HGHG. The schematic layout and principle of the self-modulation HGHG are presented in Sec. 2. In order to demonstrate the feasibility of the self-modulation HGHG for high-repetition-rate and fully coherent soft X-ray FELs, intensive numerical simulations based on the parameters of the Shanghai soft X-ray free-electron laser facility (SXFEL) are carried out in Secs. 3 and 4, respectively. We further verify that the self-modulation scheme can generate higher harmonic bunching after changing the resonance conditions of the self-modulator; the experimental results are shown in Sec. 5. The summary and prospects are given in Sec. 6.

## 2 Principle

The standard HGHG typically adopts an ultraviolet (UV) seed laser pulse to imprint a longitudinal sinusoidal energy modulation on the electron beam in a short modulator, with a periodicity of the seed laser wavelength. The following dispersive chicane is used for the associated longitudinal density modulation, which can be defined as the bunching factor. The $n$'th harmonic bunching factor can be written as[13]

$$b_n = |J_n(nAB)| \exp\left(-\frac{n^2B^2}{2}\right), \tag{1}$$

where $A = \Delta\gamma/\sigma_\gamma$, $\gamma$ is the beam energy in units of $mc^2$, $\Delta\gamma$ is the energy modulation amplitude, and $\sigma_\gamma$ is the uncorrelated energy spread. $B = kR_{56}\sigma_\gamma/\gamma$ is the dimensionless dispersion parameter, $R_{56}$ is the dispersion strength of the chicane, $k$ is the wavenumber of the seed laser, $n$ is the harmonic number, and $J_n$ is the $n$'th order first-class Bessel function. Equation (1) shows that the bunching factor decreases exponentially with the rise of harmonic number $n$. To obtain the maximum bunching factor at the $n$'th harmonic of the seed laser, a large $A$ is required, and $B$ should be optimized simultaneously. Generally, the $\Delta\gamma$ should be $n$ times larger than $\sigma_\gamma$. However, the energy spread effects induced by the seed laser limits its access to the higher harmonic number, e.g., larger than the FEL Pierce parameter $\rho$ when the FEL process cannot gain exponentially in the following radiators. The total energy spread $\sigma_{\gamma'}$ at the entrance of radiators can be written as $\sigma_{\gamma'} = \sqrt{\sigma_\gamma^2 + \Delta\gamma^2/2}$.[45] From the notation of Ref. 46, the FEL Pierce parameter is derived as

$$\rho = \left[\frac{1}{8\pi}\frac{I}{I_A}\left(\frac{K[JJ]_1}{1+K^2/2}\right)^2\frac{\gamma\lambda^2}{2\pi\sigma_x^2}\right]^{1/3}, \tag{2}$$

where $K$ is the undulator parameter, $[JJ]_1$ is the Bessel function factor associated with a planar undulator, $\lambda$ is the FEL resonant wavelength, $I_A$ is the Alfvén current, $I$ is the peak current of the electron beam, and $\sigma_x$ is the root mean square (RMS) transverse beam size. Consequently, the maximum harmonic upconversion of the standard HGHG is typically limited to 15 under the constraint of satisfying both large energy modulation and the requirement on high-gain FELs. In order to obtain shorter wavelengths, a cascading multistage scheme can be adopted, in which the FEL output of the first stage HGHG is used as the seed laser for the next.[14] The cascaded HGHG is more sensitive to beam imperfections, which, in practice, is challenging to operate at the shorter wavelength.[20,21]

Furthermore, the bunching factor versus $A$ at various harmonic numbers is illustrated in Fig. 1, according to Eq. (1). Under a particular $A$, each line represents the maximum achievable bunching factor at the optimal $R_{56}$. For instance, inducing a relatively small energy modulation $A = 2$, the maximum bunching factor of the fundamental, second, and third harmonics are 0.43, 0.22, and 0.10, respectively. The fundamental wavelength contains a significant bunching factor under this weak energy modulation, which means that further amplification can produce coherent energy modulation and reduce the requirement for the seed laser power toward high-repetition-rate FELs.[30] In addition, it can be shown that if $A$ increases, such as to 4, the bunching factors of the fundamental, second, and third harmonics increase

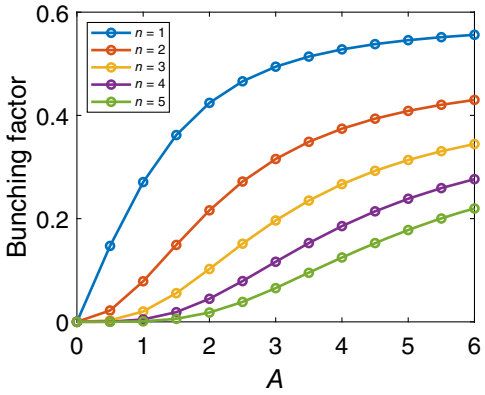


**Fig. 1** Bunching factor versus energy modulation amplitude $A$ at various harmonic numbers. Each line corresponds to the maximum bunching factor at the optimal dispersion strength.

to 0.55, 0.37, and 0.27, respectively. The bunching factor of the fundamental and second harmonics increases by 28% and 68%, respectively, whereas the third harmonic increases by a factor of 1.7. Therefore, we can amplify the initial laser-induced energy modulation at the second, third, or higher harmonics toward short-wavelength seeded FELs.[33] The schematic layout of the self-modulation HGHG setup is shown in Fig. 2. Compared with the standard HGHG, the self-modulation HGHG includes an extra chicane and a short undulator, the so-called self-modulator, which is used to reduce the initial requirements on the seed laser power significantly. A UV seed laser is utilized to interact with the electron beam in the first modulator and then generates a relatively weak energy modulation. After passing through the first chicane, the energy modulation of the electron beam is converted into longitudinal density modulation leading to a prebunched beam. Then the laser-induced energy modulation is further amplified in the self-modulator. Moreover, optimizing the dispersion strength of the second chicane can achieve a more prominent bunching factor at a higher harmonic of the seed laser in the following amplifier. It should be noted that the external seed laser is separated from the dispersive section between the modulators. This scheme is very compatible with existing seeding beamlines of FEL facilities because it is similar to the EEHG setup. The energy modulation amplitude induced in the first modulator $A_1 = \Delta\gamma_1/\sigma_\gamma$ and enhanced in the self-modulator $A_2 = \Delta\gamma_2/\sigma_\gamma$ should be analyzed and optimized with two dispersive chicanes' $R_{56}^1$ and $R_{56}^2$ simultaneously. The enhanced coherent energy modulation amplitude is calculated with the energy spread at the exit of the self-modulator. According to the theory of seeded FELs,[13] the gain process consists of three regimes: the coherent harmonic generation (CHG) with quadratic growth, exponential growth, and saturation. The CHG radiation can be generated in the self-modulator, whose total length is around two gain lengths, where $L_g \equiv \lambda_u/4\pi\sqrt{3}\rho$ is the one-dimensional (1D) gain length, with the undulator period $\lambda_u$ and the FEL Pierce parameter $\rho$ given by Eq. (2). In the CHG regime, the harmonic electric field grows linearly along the self-modulator length $z$, and the power grows quadratically along $z$. At the entrance of the self-modulator, the prebunched beam contains high harmonic components. Thereby, the self-modulator can enhance the CHG radiation. Assuming the electron beam is characterized by a uniform longitudinal distribution, the CHG power can be written as[45]

$$P_{\mathrm{coh}} = \frac{Z_0 (K[JJ]_1 \eta L_g I b_{m1})^2}{32\pi\sigma_x^2\gamma^2}, \tag{3}$$

where $Z_0 = 377\ \Omega$ is the vacuum impedance, $L_{m2}$ is the length of the self-modulator, $\eta = L_{m2}/L_g$ is the modulator scaling factor, $b_{m1}$ is the bunching factor on the resonant wavelength of the self-modulator obtained from the prebunched beam, and the other variables follow the same notation as in Eq. (2). Generally, assuming a Gaussian external seed laser interacts with the electron beam in the modulator undulator, we can obtain the amplitude of the energy modulation as (see Ref. 47)

$$\Delta\gamma(r) = \sqrt{\frac{P}{P_0}}\frac{K[JJ]_1 L_u}{\gamma\sigma_r}\ \exp\left(-\frac{r^2}{4\sigma_r^2}\right), \tag{4}$$

where $P$ is the peak power of the external seed laser, $P_0 = I_A mc^2/e \approx 8.7$ GW, $r$ is the radial position of the electron beam, and $\sigma_r$ is the RMS laser spot size in the modulator undulator. The laser spot size $\sigma_r$ should be as comparable as possible to the electron beam size $\sigma_x$ to obtain the maximum energy modulation $\Delta\gamma(0)$. However, to satisfy the transverse overlap between the electron beam and external seed laser, the laser spot size should be larger than the beam size, in the order of hundreds and tens of micrometers, respectively. The energy modulation process of the self-modulator is similar to that of the conventional modulator with an external seed laser, as it is the coherent energy modulation process generated by the CHG radiation that requires a modification to Eq. (4). Assuming that the electric field strength at the exit of the self-modulator is $E_{\mathrm{coh}}$, the coherent energy modulation process of the self-modulator can be regarded as modulated by the seed laser with an electric field strength of $E_{\mathrm{coh}}/2$ corresponding to the peak power of $P_{\mathrm{coh}}/4$. Meanwhile, for simplicity, we can assume that the spot size of the CHG radiation is larger than the beam size in the

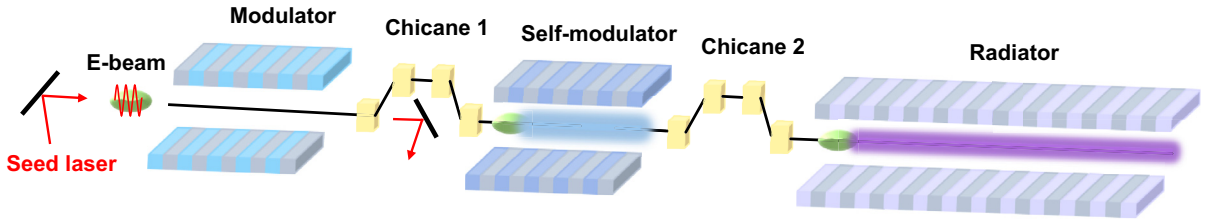


**Fig. 2** Schematic layout of the self-modulation HGHG setup. A self-modulation HGHG includes extra dispersive chicane and self-modulator, further amplifying laser-induced energy modulation to obtain a higher harmonic bunching factor.

self-modulator and that both are independent of each other. The energy modulation in the self-modulator can be simplified. Thus the modified maximum energy modulation $\Delta\gamma$ can be rewritten as

$$\Delta\gamma = \sqrt{\frac{P_{\mathrm{coh}}}{4P_0}}\frac{K[JJ]_1 L_u}{\gamma\sigma_r'}, \tag{5}$$

where $\sigma_r'$ is the equivalent spot size of the CHG radiation.

Here the critical parameters of the self-modulation HGHG are described for design and optimization. From Eqs. (4) and (5), it is clear that $A_2 \propto \sqrt{P_{\mathrm{coh}}}$ and $A_1 \propto \sqrt{P_{\mathrm{seed}}}$, where $P_{\mathrm{seed}}$ is the external seed laser power in the first modulator. As shown in Fig. 1, since $A$ is generally larger than 2, the harmonic bunching factor can be roughly considered proportional to the square root of $A$. The harmonic bunching factor $b_{m2}$ at the entrance of radiators can be simplified as $b_{m2} \propto \sqrt{A_2}$. $A_1$ is typically lower than 2, which can be roughly estimated as proportional to the bunching factor $b_{m1} \propto A_1$. Consequently, the scaling harmonic bunching factor can be easily derived as

$$b_{m2} \propto \frac{\eta^{1/2} I^{1/3} P_{\mathrm{seed}}^{1/4}}{\sigma_x^{1/6}}. \tag{6}$$

Equation (6) illustrates the scaling relationship between the harmonic bunching factor and critical parameters, such as the modulator scaling factor $\eta$, peak current $I$, peak power of the external seed laser $P_{\mathrm{seed}}$, and the electron beam size $\sigma_x$, which can *a priori* estimate the seed laser power of the self-modulation HGHG under different electron beams and undulator characteristics. For example, in the nominal case with beam size $\sigma_{x0}$, peak current $I_0$, seed laser power $P_{\mathrm{seed0}}$, and modulator scaling factor $\eta = 2$, then the $b_{m2}$ is obtained. When the beam size is reduced by half of $\sigma_{x0}/2$ and the peak current remains $I_0$, producing the same bunching factor as $b_{m2}$, the seed laser power is only $P_{\mathrm{seed}}/4$, corresponding to $\eta = 3.18$; for comparison, when the peak current is doubled to $2I_0$ and the beam size remains $\sigma_{x0}$, producing the same $b_{m2}$, the seed laser power is also reduced to $P_{\mathrm{seed}}/4$, corresponding to $\eta = 2.52$. Note that the scaling bunching factor contains three preconditions: (1) the modulator scaling factor should generally be $\lesssim 3$, according to Eq. (3); (2) the spot size of CHG radiation in the self-modulator is independent of the beam size, according to Eq. (5); and (3) the energy modulation amplitude of the first modulator is weak, typically $<2$. Therefore, during design and optimization of the self-modulation HGHG, the seed laser power requirement can be significantly reduced by optimizing the peak current and beam size, and this process is substantially achieved by reducing the gain length in the self-modulator. In practice, the length of the modulator undulator cannot be adjusted arbitrarily, thereby optimizing the electron beam quality and the focus-drift-defocus-drift (FODO) cell of the modulators is a more feasible method for the self-modulation scheme.

## 3 Toward High Repetition Rates

To investigate the principle and limits of the self-modulation HGHG, simulations were carried out by GENESIS[48] utilizing the main electron beam parameters of the SXFEL user facility (SXFEL-UF) listed in Table 1. The SXFEL-UF is aimed at generating soft X-ray pulses toward the water window around 2.3 to 4.4 nm, which contains the SASE and the seeding beamlines.[49,50] The baseline design initially considers the single-stage EEHG and the cascaded EEHG–HGHG configurations. A 266-nm seed laser with a peak power of several hundred megawatts and a repetition rate of 10 Hz is adopted. Toward high-repetition-rate FELs, the peak power requirements of external seed lasers should be further reduced to circumvent the limitations of the state-of-the-art laser system. In addition, it is currently challenging to achieve a harmonic upconversion number of externally seeding schemes to above 100 toward short-wavelength FELs. We employ SXFEL-UF electron beam parameters as a nominal case to further demonstrate the performance and application potential of the self-modulation scheme in terms of high-repetition-rate and short-wavelength FELs.

**Table 1** Main electron beam parameters of the SXFEL-UF.

| Parameter | Value | Unit |
|---|---|---|
| Beam energy | 1.4 | GeV |
| Slice energy spread | 50 | keV |
| Normalized emittance | 1 | mm·mrad |
| Bunch charge | 600 | pC |
| Bunch length (FWHM) | 800 | fs |
| Peak current (Gaussian) | 700 | A |
| Beam size (RMS) | 100 | $\mu$m |

As described in Sec. 2, the modulator scaling factor $\eta$, peak current $I$, seed laser power $P_{\mathrm{seed}}$, and the electron beam size $\sigma_x$ are critical for high-repetition-rate FELs. The beam size is reduced to 50 $\mu$m from the nominal case of 100 $\mu$m to compare the effect of beam size on the self-modulation HGHG. In addition, the peak current is increased to 1400 A for the nominal case of 700 A to compare the effect of the peak current further. It should be noted that a constant self-modulator length of 1.6 m is here considered, whereas the modulator scaling factor $\eta$ is changed accordingly.

To reasonably compare the effects of beam size and peak current on self-modulation HGHG efficiency, the same target bunching factor of 8% is used in all cases in this section. The harmonic bunching factor is obtained at the entrance of radiators for the 8th to 15th harmonics of the seed laser. The parameters of the FODO lattice in the following radiators are kept at the same value. The steady-state simulations are carried out with the electron and undulator parameters listed in Tables 1 and 2 to optimize working points of the self-modulation HGHG fast, i.e., the seed laser power and dispersion strength.

The seed laser power ratio represents the ratio of the seed laser power of standard HGHG to that of the self-modulation HGHG, as shown in Fig. 3. One can find that the seed laser ratio is a function of the harmonic number. In the nominal case, the seed laser power for the eighth harmonic of the seed laser can be reduced by a factor of 237 and decreases as the number of harmonics increases. Figure 3 clearly shows that the beam size and peak current can further reduce the seed laser requirement and enhance the performance of the self-modulation scheme, resulting in a reduction of the seed laser power by up to nearly 3 orders of magnitude. More importantly, in the nominal case, the Pierce parameter of the self-modulator that resonates at the fundamental wavelength of the seed laser is calculated to

**Table 2** Main simulation parameters of the seed laser and the undulators.

| Parameter | Value | Unit |
|---|---|---|
| **Seed laser** | | |
| Wavelength | 266 | nm |
| Peak power (standard HGHG) | 17 to 75 | MW |
| Peak power (self-modulation HGHG) | 0.019 to 1.6 | MW |
| Pulse duration (FWHM) | 150 | fs |
| Rayleigh length | 5 | m |
| Spot size (RMS) | 325 | $\mu$m |
| **Modulator** | | |
| $K$ | 9.891 | |
| Period | 8 | cm |
| Length | 1.6 | m |
| **Self-modulator** | | |
| $K$ | 5.593 to 9.891 | |
| Period | 8 | cm |
| Length | 1.6 or 2 | m |
| **Radiator** | | |
| $K$ | 1.823 to 4.239 | |
| Period | 5 | cm |
| Length | 3 | m |

$\rho = 4.6 \times 10^{-3}$, corresponding to the 1D gain length of 0.80 m and the modulator scaling factor $\eta = 2$. Similarly, the 1D gain length of the second and third cases is calculated to be 0.51 and 0.63 m, corresponding to the modulator scaling factor of 3.16 and 2.52, respectively. According to Eq. (6), the fourfold scaling curve obtained by the nominal case is shown in Fig. 3. Since the three-dimensional (3D) effect and the additional energy modulation introduced by the CHG radiation spot size in the self-modulator are neglected in the roughly estimated Eq. (6), the second case shows that the ratio is poorly conformed at higher harmonics; the third case shows that the ratio is better conformed, but with a slight increase on higher harmonics over 12th harmonics. Therefore, the effect of beam size $\sigma_x$ and peak current $I$ can still be estimated roughly by Eq. (6), and modulator scaling factor $\eta$ is an intermediate variable during the design and optimization of self-modulation HGHG. In addition, the energy spread ratio represents the ratio of the energy spread of standard HGHG to that of the self-modulation HGHG at the entrance of radiators, as shown in Fig. 4. Because of CHG radiation in the self-modulator, the energy spread of self-modulation HGHG is inherently larger than that of standard HGHG. Figure 4 shows that decreasing the beam size reduces the seed laser requirement at a low-energy spread cost compared to increasing the peak current, which is more noticeable at higher harmonics. Furthermore, increasing the peak current introduces a larger energy spread than the nominal case. However, the difference is not evident at higher harmonics. In terms of practicability, reducing the beam size is a more efficient way to loosen the seed laser power demand in the self-modulation scheme.

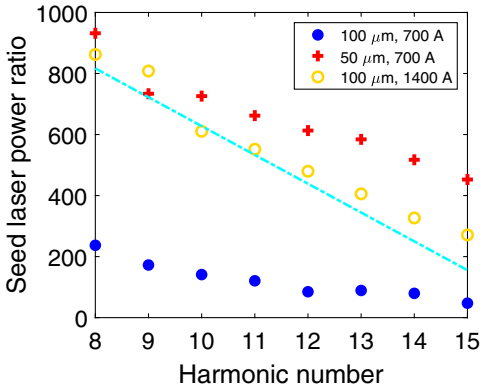


**Fig. 3** The seed laser power ratio of the standard HGHG and self-modulation HGHG in different cases. The blue dot, red cross, and yellow circle correspond to the nominal case of beam size of 100 $\mu$m and peak current of 700 A, the second case of beam size of 50 $\mu$m and peak current of 700 A, and the third case of 100 $\mu$m and 1400 A, respectively. The dotted line corresponds to the scaling curve.

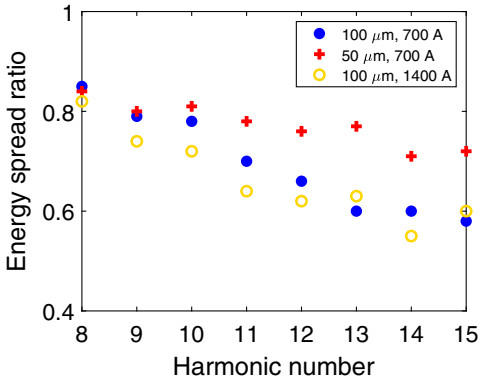


**Fig. 4** The energy spread ratio of the standard HGHG and self-modulation HGHG in different cases. The blue dot, red cross, and yellow circle correspond to the nominal case of beam size of 100 $\mu$m and peak current of 700 A, the second case of beam size of 50 $\mu$m and peak current of 700 A, and the third case of 100 $\mu$m and 1400 A, respectively.

To evaluate the reduction of the seed laser power requirement, we carry out an example analysis of self-modulation HGHG at the 13th harmonic of the seed laser. Initially, in the case of 100 and 50 $\mu$m beam sizes, we introduce an optimal energy modulation in the first modulator by a 266-nm seed laser with peak power of 0.62 and 0.085 MW to the initial energy modulation $A_1$ of 1.2 and 0.6, respectively. The beam size is reduced by half, corresponding to a 7.3-fold reduction of the seed laser power. Second, the two-dimensional scanning of the $R_{56}$ of dispersive chicanes for obtaining the 13th harmonic bunching factor of 8% in different beam sizes is shown in Fig. 5. In the case of the beam size of 100 $\mu$m, the optimal $R_{56}$ values of the first and second chicanes are 1.04 and 0.06 mm, respectively. Similarly, the optimal $R_{56}$ values of the first and second chicane in the other case are 0.92 and 0.09 mm, respectively. It is found that $R_{56}^2$ is more sensitive than $R_{56}^1$. Third, with the energy spread $\sigma_\gamma$ at the radiator entrance, the energy modulation amplitude $A_2$ can be roughly estimated by $\sqrt{2[(\sigma_{\gamma'}/\sigma_\gamma)^2 - 1]}$. In the case of the beam size of 100 $\mu$m, the energy modulation is

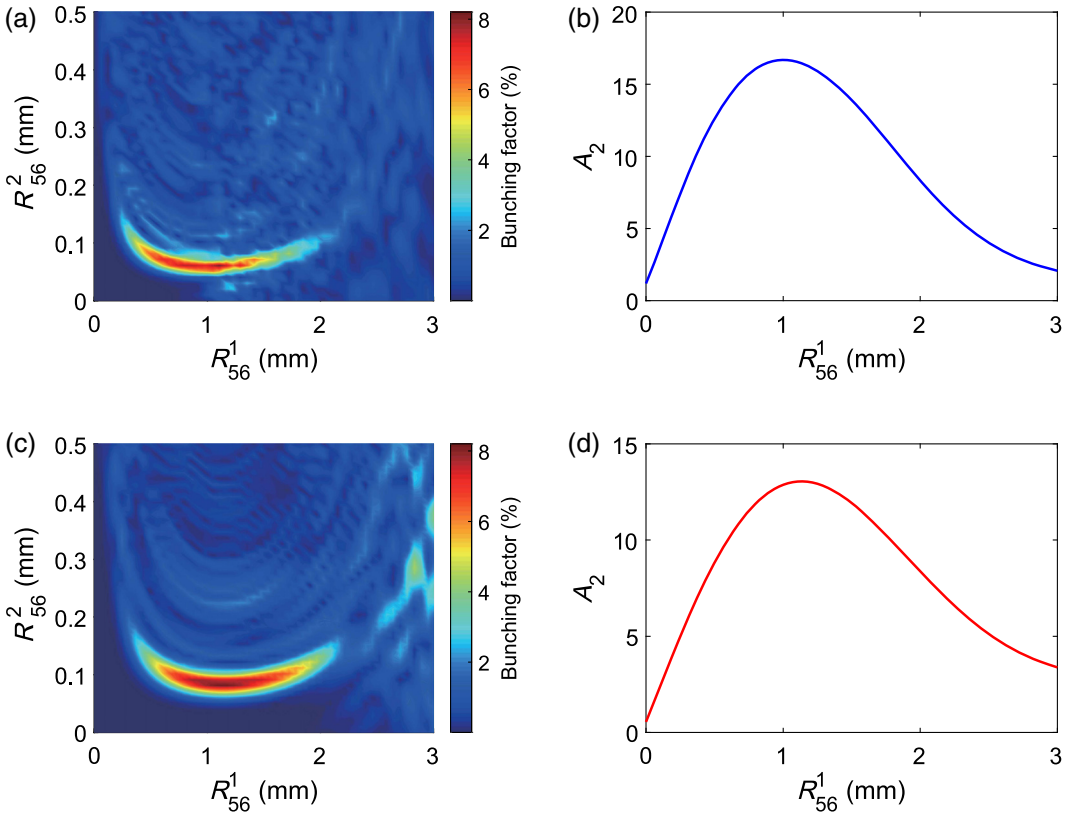


**Fig. 5** Optimization for the $R_{56}$ of two chicanes by GENESIS simulations to obtain the 13th harmonic bunching factor of 8% and corresponding energy modulation amplitude $A_2$ of the entrance of the radiator in different beam sizes. (a), (b) Beam size of 100 $\mu$m; (c), (d) beam size of 50 $\mu$m.

about 850 keV, corresponding to $A_2 = 16.7$; whereas a lower energy modulation of 650 keV is introduced in the case of the beam size of 50 $\mu$m, corresponding to $A_2 = 13.0$. The magnification efficiency of energy modulation for $A_2/A_1$ is about 13.9 and 21.7 in different beam sizes, respectively. Thus the beam size reduction can significantly relax the seed laser power requirement and increase the bunching factor's efficiency. Finally, 3D time-dependent simulations are carried out; the output FEL performance is shown in Fig. 6. We compare the performance of the self-modulation HGHG and the standard HGHG with different beam sizes: the seed laser required for the self-modulation HGHG is only a few tens of kilowatts, and the shot noise in the first modulator is about 43 W, which can be estimated by Refs. 51 and 52,

$$P_{\text{noise}} = \frac{3^{3/4} 4\pi\rho^2 P_{\text{beam}}}{N_\lambda \sqrt{\pi\eta}}, \tag{7}$$

where $P_{\text{beam}}$ is the electron beam power, and $N_\lambda$ is the number of electrons per seed laser wavelength. The signal-to-noise ratio (SNR) is significantly lower than that of the standard HGHG with the introduction of a few tens of megawatts seed lasers. For both self-modulation HGHG and standard HGHG, the saturation of the FEL power is around 0.5 GW. The pulse duration and the spectral width are similar for both cases. The slight pulse lengthening in the self-modulation HGHG can be explained by the slippage effect introduced by the self-modulator and by the fact that the bunching envelope can be changed during the amplification process. The additional broadening of the spectrum may result from the self-modulation process that changes the electron beam energy distribution and induces additional energy spread, which can also explain the appearance of spikes in the pulse temporal profiles. In the case of 100-$\mu$m beam size, the time-bandwidth product (TBP) of the standard HGHG and self-modulation HGHG, describing the longitudinal coherence of the FEL radiation, are 2.28 and 3.67, respectively. The degradation of the longitudinal coherence is in the acceptable range. In this case, the seed laser power can be easily reduced by a factor of 932 by self-modulation.

## 4 Toward Short Wavelength

Typically, short-wavelength seeded FELs are limited by two main factors: seed laser performance, such as wavelength $\lambda_s$ and peak power, and harmonic upconversion efficiency for high-gain FELs. As described in Sec. 3, the self-modulation scheme can significantly reduce the seed laser requirement. The self-modulation performance can be further optimized under a better beam envelope and different resonances of the self-modulator.[30] Moreover, the harmonic-enhanced HGHG numerically verifies that the 13.5-nm (20th harmonic) FEL radiation can be obtained by a UV seed laser.[33] To investigate the potential of the self-modulation scheme to generate ultrahigh harmonics, such as the 30th harmonic, the self-modulation HGHG is further discussed.

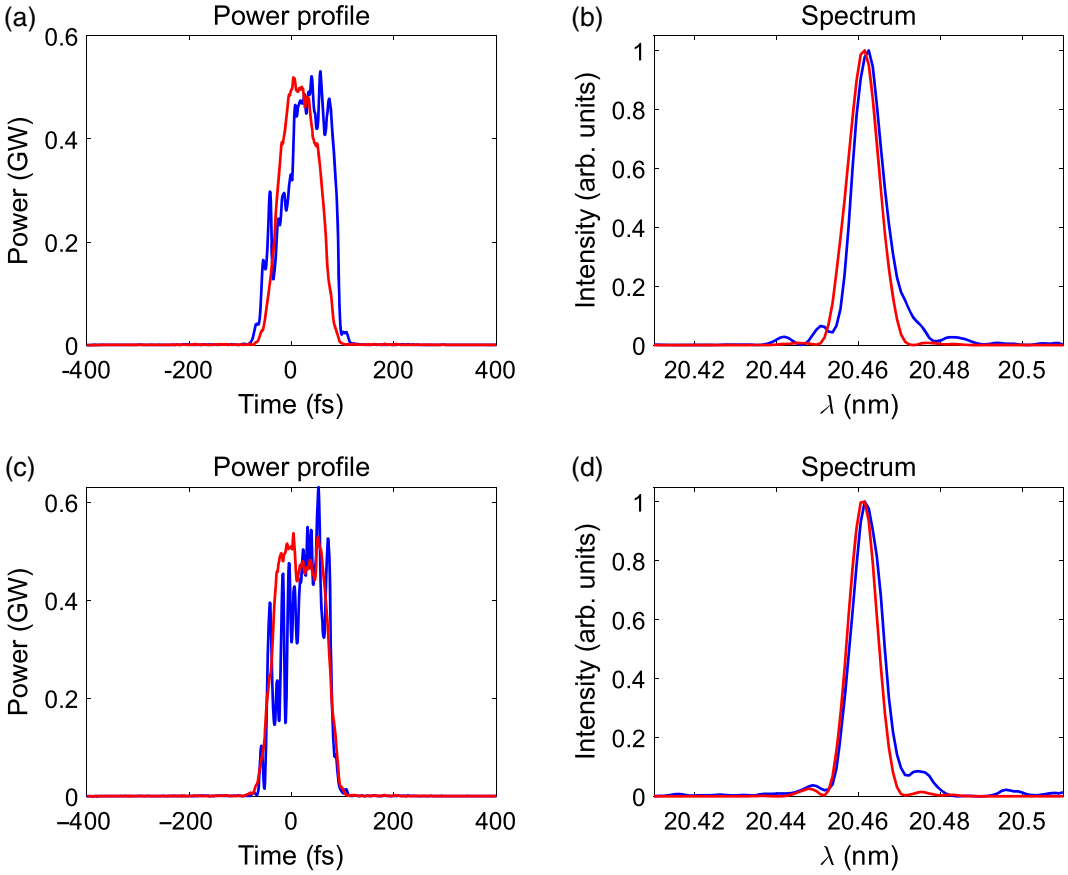


**Fig. 6** Comparison of the FEL performance between self-modulation HGHG (blue) and standard HGHG (red) at the 13th harmonic of the 266-nm seed laser in the cases of different beam sizes. (a), (b) Beam size of 100 $\mu$m; (c), (d) beam size of 50 $\mu$m.

With the parameters of the nominal case listed in Table 1, the optimization of the self-modulation scheme at SXFEL-UF toward shorter wavelengths is presented in Fig. 7. To enhance the coherent energy modulation, we increase the self-modulator length from 1.6 to 2 m in this section, corresponding to $\eta = 2.5$. To obtain an adequate bunching factor at various harmonics and improve the SNR, the initial energy modulation amplitude $A_1$ is significantly increased to 6, corresponding to the seed laser peak power of 20 MW. As shown in Fig. 7, a bunching factor larger than 5% is obtained when the self-modulator resonates at the fundamental, second, and third harmonics of the seed laser. The optimal dispersion strength $R_{56}^1$ is considered almost unchanged, and the harmonic bunching is more sensitive to the second dispersion strength $R_{56}^2$. The large energy modulation amplitude $A_2 = 40$ is obtained when the self-modulator is resonated at the fundamental wavelength. However, the energy spread is too large to generate high-gain FEL pulses in this case. In addition, a bunching factor larger than 5% can be obtained when the self-modulator resonates at the second and third harmonic, corresponding to the maximum energy modulation amplitude of 24 and 15, respectively. Figure 7 also indicates that the coherent energy modulation amplitude $A_2$ decreases significantly as the self-modulator is tuned to a higher harmonic number. Therefore, the self-modulator can resonate at a higher harmonic, generating an appropriate energy modulation with a lower energy spread.

As analyzed in Sec. 2, the self-modulator can produce a large energy modulation with a weak initial energy modulation, where the self-modulator resonates at the fundamental wavelength. Moreover, the maximum energy modulation in the self-modulation HGHG is significantly larger than that of the standard HGHG when both configurations have the same harmonic bunching factor. Due to the additional energy spread introduced by the self-modulation process, the total energy spread of the self-modulation HGHG is significantly larger than that of the standard HGHG, especially at higher harmonics (see Fig. 4). As discussed above, in the third-harmonic self-modulation, the induced energy spread is minimum, whereas the bunching at the 30th harmonic is still considerable. The 3D time-dependent simulations are carried out to verify the feasibility of the third-harmonic self-modulation. By optimizing the dispersion strength, the energy modulation can be converted into density modulation with a 30th harmonic bunching factor of 5%. As shown in Fig. 8, the longitudinal phase space of the electron beam at the radiator entrance in a self-modulation HGHG configuration is not ideally sinusoidal compared to the standard HGHG. It is worth noting that the energy modulation introduced by the third-harmonic self-modulation is less than half that of the fundamental self-modulation. Further enhancement of the initial energy modulation with resonance at higher harmonics can increase harmonic upconversion while significantly avoiding electron beam quality degradation.

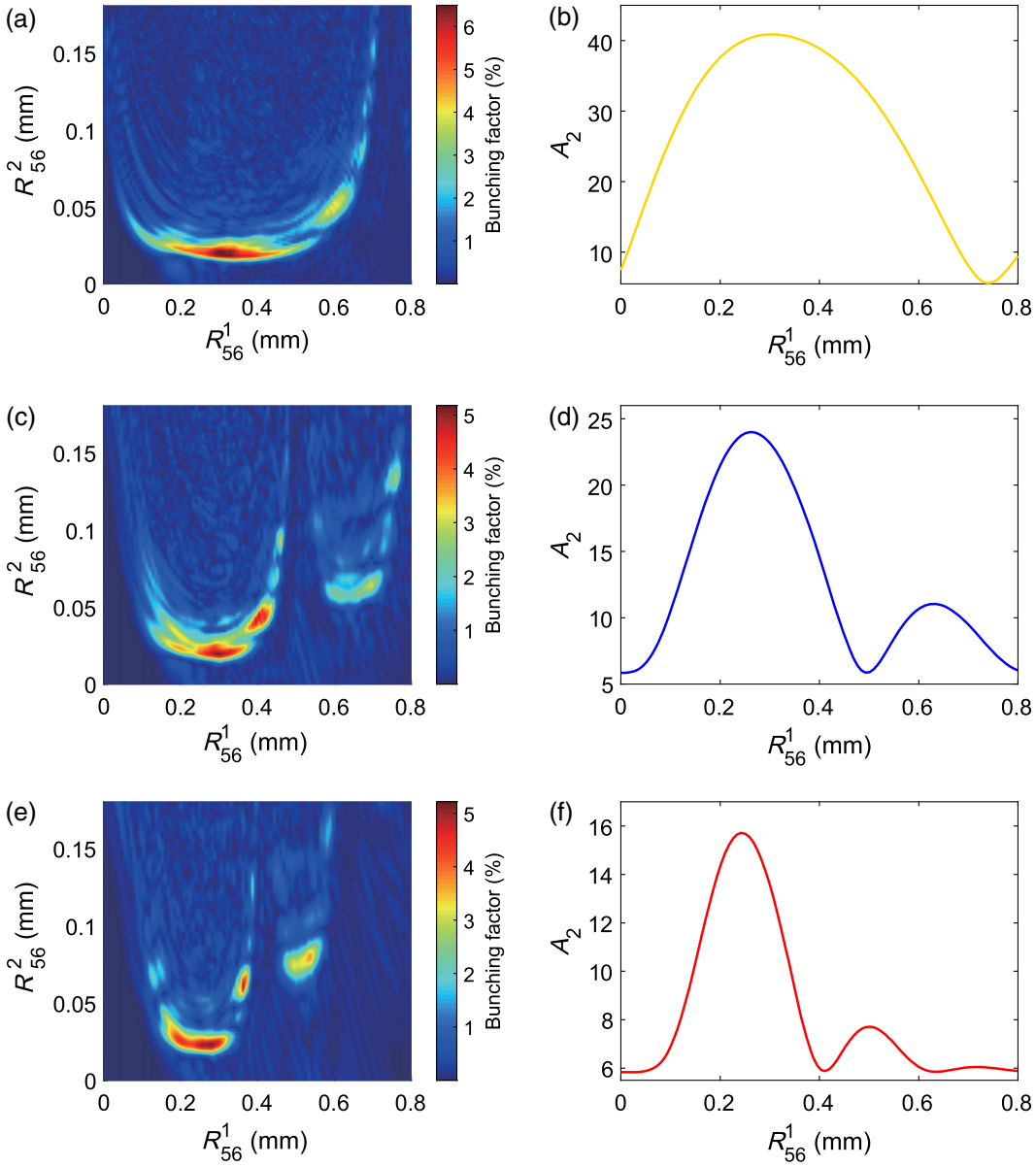


**Fig. 7** Optimization of the $R_{56}$ of two chicanes toward the 30th harmonic of the seed laser. The self-modulator resonates at (a), (b) the fundamental wavelength; (c), (d) the second; (e), (f) the third harmonics of the seed laser, respectively.

Furthermore, the output FEL gain curve, power profile, and spectrum are summarized in Fig. 9, using the SXFEL-UF parameters listed in Tables 1 and 2. The saturation pulse energy reaches 54.7 $\mu$J at the end of the radiators, with a total length of 24 m. Because of the additional slippage in the self-modulator and the pulse shortening effect in seeded FELs,[53] the final output FEL pulse length of about 153.4 fs (FWHM) is comparable to the seed laser pulse duration of 150 fs (FWHM). There are several spikes in the power profile due to the lower input seed laser power and the shot-noise effect. After six radiator modules, the maximum output peak power is increased to about 0.5 GW. The relative bandwidth (FWHM) of the final output FEL spectrum is about $1.3 \times 10^{-4}$. Thus the TBP of the 30th harmonic can be calculated to be 0.649, which is only 1.47 times the Fourier-transform limit. Consequently, the resonance of the self-modulator tuned at the third harmonic is a favorable configuration for short-wavelength FEL at SXFEL-UF.

We further analyze harmonic self-modulation in terms of the bunching factor. Figure 10 presents the bunching factor at various harmonic numbers, where the target bunching factor is the bunching factor at the 30th harmonic. The bunching factor oscillations are clearly seen due to the self-modulation that turns the energy spread distribution into a saddle shape.[54] The initial energy modulation amplitude of the first modulator is only six with a 20-MW seed laser. If no self-modulator is introduced, the maximum bunching factor at the 30th harmonic is only $5 \times 10^{-5}$, just the shot-noise level. Under the same initial energy modulation, the optimized maximum 30th harmonic bunching factor of 6.5% is not the local maximum value due to bunching factor oscillation when the self-modulator is tuned at the

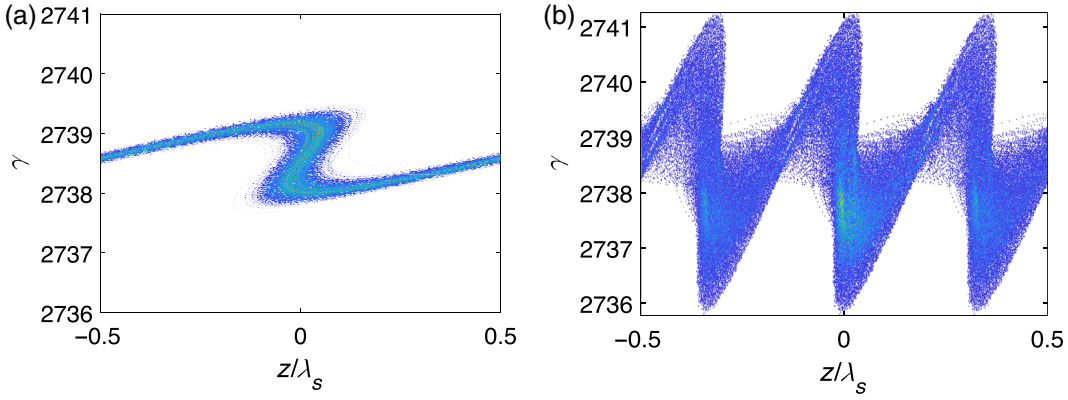


**Fig. 8** The longitudinal phase space of the electron beam in one seed laser wavelength $\lambda_s$ at the entrance of the (a) self-modulator and (b) radiator, where the self-modulator is tuned at the third harmonic of the seed laser.

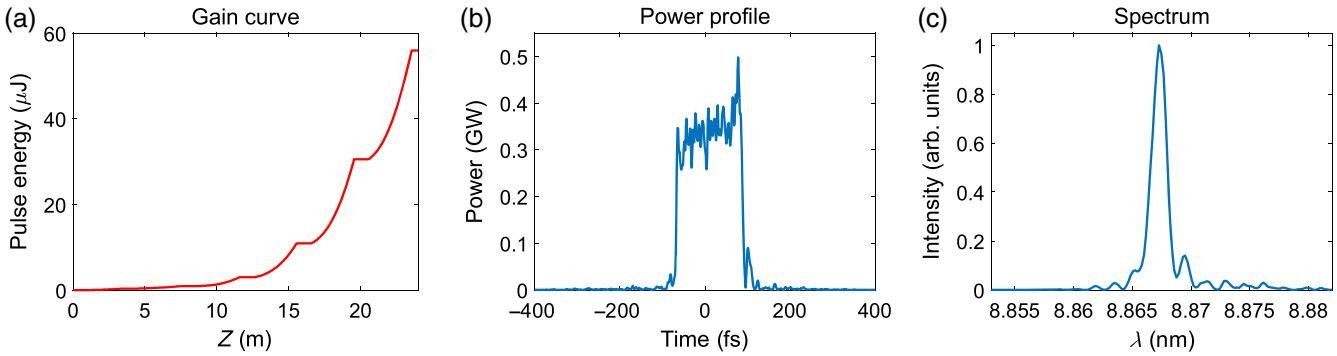


**Fig. 9** The output FEL performance at the 30th harmonic of the seed laser in the third-harmonic self-modulation. (a) 8.87-nm radiation gain curve in the radiator. (b), (c) The power profile and spectrum after six radiator modules, respectively.

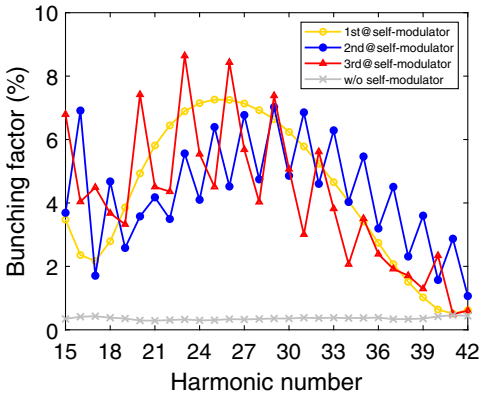


**Fig. 10** Bunching factor after the second chicane as a function of the harmonic number in various cases, including without self-modulator and the resonance of the self-modulator tuned at the fundamental wavelength, second, and third harmonic of the seed laser, respectively.

fundamental wavelength. If the self-modulator resonates at the second harmonic, the enhanced coherent energy modulation can lead to bunching enhancement of the even harmonics. However, as shown in Fig. 10, the optimal bunching factor for the 30th harmonic is close to 5% but is not the maximum bunching factor. Instead, the 29th and 31st harmonics are enhanced, reaching almost 7%. Similarly, in the third-harmonic self-modulation, the integer harmonics of 3 should be enhanced. The optimal bunching factor at the 30th harmonic is close to 5% but is not the local maximum value. The 29th and 31st harmonic bunching are enhanced to 7.5% and 5.8%, respectively. The working points in various cases are almost identical, such as the dispersion strength $R_{56}$. The electron beam has been premodulated when it enters the self-modulator. The combination of increased energy spread and the change in the energy distribution of the electron beam may lead to frequency mixing. In addition, it is possible that when the self-modulator resonates at higher harmonics, such as the third harmonic, the prebunched electron beam produces a weak harmonic energy modulation, which is slightly stronger than the initial energy modulation. The frequency components at the fundamental or second harmonic may cause a frequency mixing phenomenon. According to Fig. 1, if

the initial energy modulation amplitude $A_1$ reaches 6, the pre-bunched beam entering the self-modulator has a more significant bunching factor at the second, third, or even higher harmonics. In brief, the self-modulation HGHG can achieve a bunching factor close to 5% at the 30th harmonic, reaching the soft X-ray wavelength range, where the standard HGHG is unattainable.

## 5 Experiments

Proof-of-principle experiments were conducted in SXFEL to demonstrate the self-modulation scheme. In the previous experiment,[30] an electron beam with a laser-induced energy modulation as small as 1.8 times the slice energy spread was employed, and the initial energy modulation was enhanced threefold through the self-modulation method. Then the electron beam was used for lasing at the 7th harmonic of a 266-nm seed laser in a single-stage HGHG setup and 30th harmonic of the seed laser in a two-stage HGHG setup.

Here we further experimentally demonstrate that the change of the resonance of the self-modulator can amplify the laser-induced energy modulation and generate a high harmonic bunching. The experiment was conducted at the SXFEL test facility (SXFEL-TF),[49,50] which employs a cascaded EEHG–HGHG scheme with the "fresh bunch" technique. The schematic layout of the SXFEL-TF is displayed in Fig. 11. In the experiment, we used the modulator 1 and fresh bunch chicane of the first-stage EEHG and the modulator, dispersive section, and radiator of the second-stage HGHG to form the self-modulation HGHG. The electron beam driving the experiment has an energy of 780 MeV, bunch charge of 550 pC, peak current of 600 A, normalized emittance of 1.5 mm · mrad, and envelope size of 300 $\mu$m. The pulse length and wavelength of the seed laser were 160 fs (FWHM) and 266 nm, respectively.

As shown in Fig. 11, the external seed laser was used to modulate the electron beam at modulator 1. The dispersion strength of the first chicane was set to 0.24 mm. At first, the self-modulator was removed. The first undulator segment of radiator 2, which can contain resonances from the 4th to more than the 11th harmonic of the seed laser, was used to produce coherent radiation and thus estimate the energy modulation level. The undulator period is 40 mm. For the standard HGHG case, a relatively high-power seed laser is used, in which case coherent radiation at more than the sixth harmonic can be detected. To ensure a weak seed laser power in the experiment, we continuously attenuated the seed laser intensity until the 4th harmonic signal could not be detected. In this case, the energy modulation amplitude was estimated as below 4 times the slice energy spread.

Subsequently, the resonance of the self-modulator was tuned at the second harmonic of the seed laser. The dispersion strength of the second chicane was set to a reasonable range to obtain a large harmonic bunching factor. We targeted the 7th harmonic of the seed laser and precisely optimized the dispersion strength $R_{56}$ of the second chicane from 0.029 to 0.055 mm and simultaneously scanned the gap of the undulator segment to obtain coherent radiation signals at various harmonic numbers. Figure 12(a) displays the measured coherent radiation intensity at various harmonic numbers, setting the dispersion strength of the second chicane to the optimal value of 0.038 mm at the seventh harmonic. The coherent radiation can be detected at up to the 11th harmonic, i.e., 24.2 nm. Furthermore, we slightly increased the dispersion strength of the first chicane to 0.28 mm for comparison. Similarly, we scanned the dispersion strength of the second chicane from 0.029 to 0.055 mm and the gap of the undulator segment to contain resonances from the 4th to 12th harmonic of the seed laser. When we considered the 6th harmonic of the seed laser as the target wavelength, we found that the optimal chicane dispersion strength was 0.048 mm, as shown in Fig. 12(b). The coherent radiation can be detected at even the 12th harmonic. Since the external seed laser does not directly introduce the coherent energy modulation, and the self-modulator resonates at the second harmonic, it is challenging to measure the energy modulation amplitude $A_2$ at the exit of the self-modulator through the coherent radiation-based method.[55] Although the differences in the coherent radiation signals at different dispersions may appear small, the optimal dispersion strengths are critical for achieving the best lasing performance, especially at higher harmonics. Moreover, compared with the previous experiment [see Fig. 3(a) in Ref. 30], the bunching performance is better than the case with an energy modulation amplitude of 6 times the slice energy spread enhanced by a 266-nm radiation.

In addition, we experimentally observed the frequency-mixing phenomenon, which may result in odd harmonic signals being stronger than even harmonic ones, as shown in Fig. 12. Because the initial energy modulation at the fundamental wavelength introduces a relatively large energy spread, the energy distribution of the electron beam is changed. After the harmonic self-modulation process, the energy spread increases, and the energy distribution of the electron beam is changed again while generating a high-frequency component that may lead to the frequency shift at the higher harmonics. Moreover, the dispersion strength of the first chicane may not be optimal, resulting in a weak harmonic energy modulation in the self-modulator, which is comparable to the initial laser-induced energy modulation. The bunching at the fundamental wavelength

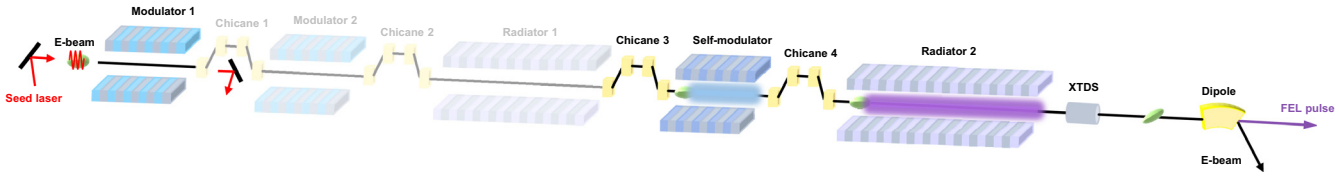


**Fig. 11** The typical setup of the SXFEL-TF adopted a cascaded EEHG–HGHG scheme. In the self-modulation experiment, modulator 1, with a period of 80 mm in the first stage EEHG, was used as the first modulator. Chicane 3 is the fresh bunch chicane used as the first chicane. A modulator of the second stage HGHG with a period of 55 mm was the self-modulator. Chicane 4 was regarded as the second chicane. X-band transverse deflection structure (XTDS) section was used to measure the longitudinal phase space of the electron beam.

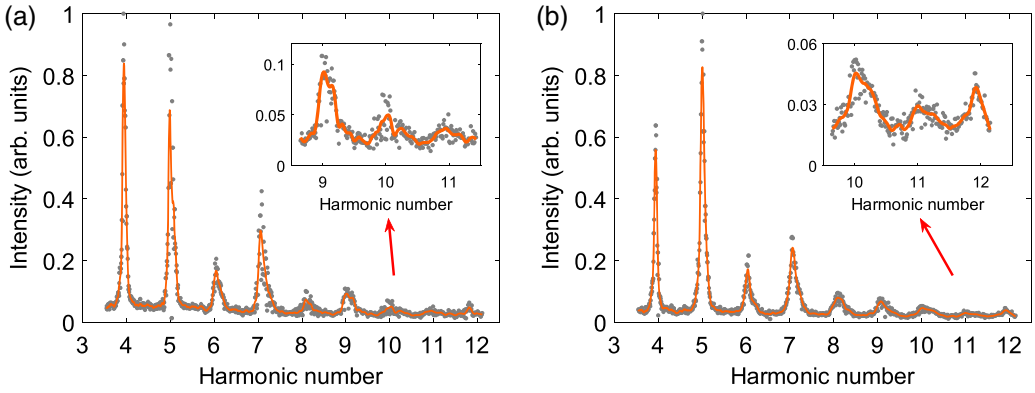


**Fig. 12** The measured intensity of the coherent radiation at various harmonic numbers in the first undulator segment of the radiator, under different $R_{56}$ values of the second chicane of (a) 0.038 mm and (b) 0.048 mm, respectively. The points represent the measurement results, and the curve represents the envelope obtained by smoothing the measurement data.

of the prebunched beam is maintained, which in combination with the energy modulation of the second harmonic, leads to frequency mixing.

In brief, we observed coherent radiation signals up to the 11th and even the 12th harmonic in both cases, confirming the effectiveness of harmonic self-modulation in amplifying the laser-induced energy modulation. Moreover, harmonic self-modulation holds the promise of realizing shorter wavelength FELs by reasonably optimizing the electron-beam orbit, the initial weak energy modulation, the resonance condition of the self-modulator, and the dispersion strength of chicanes.

## 6 Summary and Prospects

In summary, numerical simulations are presented to demonstrate that the self-modulation scheme can relax the requirement of the seed laser power by around 3 orders of magnitude in a seeded FEL, and the self-modulation HGHG is promising to lase at the 30th harmonic of the seed laser. In addition, we experimentally demonstrate that the harmonic self-modulation can amplify the initial laser-induced energy modulation, which is an essential step in future experimental studies of the self-modulation scheme.

These results further suggest that self-modulation is very promising for realizing high-repetition-rate seeded FELs, which are expected to show great promise for multidimensional coherent spectroscopies. The self-modulation can also facilitate schemes that require high-power laser systems.[56–58] Moreover, this scheme makes it possible for those light sources with short wavelengths but low-peak power, such as the high-harmonic generation,[59–61] to be used as seeding sources for FELs to achieve shorter wavelengths.

### Acknowledgments

The authors would like to thank W. J. Fan, N. S. Huang, Z. Wang, D. Gu, and C. Feng for their helpful discussions and comments. This work was supported by the CAS Project for Young Scientists in Basic Research (Grant No. YSBR-042), the National Natural Science Foundation of China (Grant Nos. 12125508 and 11935020), the Program of Shanghai Academic/Technology Research Leader (Grant No. 21XD1404100), and the Shanghai Pilot Program for Basic Research of the Chinese Academy of Sciences, Shanghai Branch (Grant No. JCYJ-SHFY-2021-010).

### Data, Materials, and Code Availability

The data that support the findings of this study are available from the corresponding author upon reasonable request.

### References

1. C. Pellegrini, A. Marinelli, and S. Reiche, "The physics of X-ray free-electron lasers," *Rev. Mod. Phys.* **88**, 015006 (2016).
2. N. Huang et al., "Features and futures of X-ray free-electron lasers," *Innovation* **2**(2), 100097 (2021).
3. L. Serafini et al., "MariX, an advanced MHz-class repetition rate X-ray source for linear regime time-resolved spectroscopy and photon scattering," *Nucl. Instrum. Methods Phys. Res., Sect. A* **930**, 167–172 (2019).
4. P. Emma et al., "First lasing and operation of an ångstrom-wavelength free-electron laser," *Nat. Photonics* **4**, 641–647 (2010).
5. T. Ishikawa et al., "A compact X-ray free-electron laser emitting in the sub-ångström region," *Nat. Photonics* **6**, 540–544 (2012).
6. H. S. Kang et al., "Hard X-ray free-electron laser with femtosecond-scale timing jitter," *Nat. Photonics* **11**, 708–713 (2017).
7. W. Decking et al., "A MHz-repetition-rate hard X-ray free-electron laser driven by a superconducting linear accelerator," *Nat. Photonics* **14**, 391–397 (2020).
8. E. Prat et al., "A compact and cost-effective hard X-ray free-electron laser driven by a high-brightness and low-energy electron beam," *Nat. Photonics* **14**, 748–754 (2020).
9. A. M. Kondratenko and E. L. Saldin, "Generating of coherent radiation by a relativistic electron beam in an ondulator," *Part. Accel.* **10**, 207–216 (1980).
10. R. Bonifacio et al., "Spectrum, temporal structure, and fluctuations in a high-gain free-electron laser starting from noise," *Phys. Rev. Lett.* **73**, 70–73 (1994).
11. J. Feldhaus et al., "Possible application of X-ray optical elements for reducing the spectral bandwidth of an X-ray SASE FEL," *Opt. Commun.* **140**(4), 341–352 (1997).
12. G. Geloni, V. Kocharyan, and E. Saldin, "A novel self-seeding scheme for hard X-ray FELs," *J. Mod. Opt.* **58**(16), 1391–1403 (2011).
13. L. H. Yu, "Generation of intense UV radiation by subharmonically seeded single-pass free-electron lasers," *Phys. Rev. A* **44**(8), 5178–5193 (1991).

14. L. H. Yu and I. Ben-Zvi, "High-gain harmonic generation of soft X-rays with the 'fresh bunch' technique," *Nucl. Instrum. Methods Phys. Res., Sect. A* **393**(1–3), 96–99 (1997).
15. G. Stupakov, "Using the beam-echo effect for generation of short-wavelength radiation," *Phys. Rev. Lett.* **102**(7), 074801 (2009).
16. D. Xiang and G. Stupakov, "Echo-enabled harmonic generation free electron laser," *Phys. Rev. Spec. Top.—Accel. Beams* **12**, 030702 (2009).
17. H. Deng and C. Feng, "Using off-resonance laser modulation for beam-energy-spread cooling in generation of short-wavelength radiation," *Phys. Rev. Lett.* **111**(8), 084801 (2013).
18. L. H. Yu, "High-gain harmonic-generation free-electron laser," *Science* **289**(5481), 932–934 (2000).
19. E. Allaria et al., "Highly coherent and stable pulses from the FERMI seeded free-electron laser in the extreme ultraviolet," *Nat. Photonics* **6**, 699–704 (2012).
20. E. Allaria et al., "Two-stage seeded soft-X-ray free-electron laser," *Nat. Photonics* **7**, 913–918 (2013).
21. B. Liu et al., "Demonstration of a widely-tunable and fully-coherent high-gain harmonic-generation free-electron laser," *Phys. Rev. ST Accel. Beams* **16**, 020704 (2013).
22. Z. T. Zhao et al., "First lasing of an echo-enabled harmonic generation free-electron laser," *Nat. Photonics* **6**, 360–363 (2012).
23. E. Hemsing et al., "Echo-enabled harmonics up to the 75th order from precisely tailored electron beams," *Nat. Photonics* **10**, 512–515 (2016).
24. P. R. Ribič et al., "Coherent soft X-ray pulses from an echo-enabled harmonic generation free-electron laser," *Nat. Photonics* **13**, 555–561 (2019).
25. C. Feng et al., "Coherent extreme ultraviolet free-electron laser with echo-enabled harmonic generation," *Phys. Rev. Accel. Beams* **22**, 50703 (2019).
26. J. Stohr, "Linac coherent light source II (LCLS-II) conceptual design report," (No. SLAC-R-978). SLAC National Accelerator Lab., Menlo Park, California (2011), https://doi.org/10.2172/1029479.
27. Z. Zhao et al., "SCLF: an 8-GeV CW SCRF Linac-based X-ray FEL facility in Shanghai," in Proc. of Int. Free Electron Laser Conf. (FEL'17), JACoW, Geneva, Switzerland, pp. 182–184 (2018).
28. N.-S. Huang et al., "The MING proposal at shine: megahertz cavity enhanced X-ray generation," *Nucl. Sci. Tech.* **34**, 6 (2023).
29. W. Ackermann et al., "Operation of a free-electron laser from the extreme ultraviolet to the water window," *Nat. Photonics* **2**(6), 336–342 (2007).
30. J. Yan et al., "Self-amplification of coherent energy modulation in seeded free-electron lasers," *Phys. Rev. Lett.* **126**, 084801 (2021).
31. J. Yan et al., "First observation of laser–beam interaction in a dipole magnet," *Adv. Photonics* **3**(4), 045003 (2021).
32. G. Paraskaki et al., "High repetition rate seeded free electron laser with an optical klystron in high-gain harmonic generation," *Phys. Rev. Accel. Beams* **24**, 120701 (2021).
33. S. Zhao, W. Qin, and S. Huang, "Harmonic-enhanced high-gain harmonic generation for a high repetition rate free-electron laser," *High Power Laser Sci. Eng.* **10**, e4 (2022).
34. P. Gandhi et al., "Oscillator seeding of a high gain harmonic generation free electron laser in a radiator-first configuration," *Phys. Rev. ST Accel. Beams* **16**, 020703 (2013).
35. K. Li and H. Deng, "Gain cascading scheme of a free-electron-laser oscillator," *Phys. Rev. Accel. Beams* **20**(11), 110703 (2017).
36. N. S. Mirian et al., "High-repetition rate and coherent free-electron laser in the tender x rays based on the echo-enabled harmonic generation of an ultraviolet oscillator pulse," *Phys. Rev. Accel. Beams* **24**, 050702 (2021).
37. M. Opromolla et al., "High repetition rate and coherent free-electron laser oscillator in the tender X-ray range tailored for linear spectroscopy," *Appl. Sci.* **11**(13), 5892 (2021).
38. S. Ackermann et al., "Novel method for the generation of stable radiation from free-electron lasers at high repetition rates," *Phys. Rev. Accel. Beams* **23**, 71302 (2020).
39. V. Petrillo et al., "Coherent, high repetition rate tender X-ray free-electron laser seeded by an extreme ultra-violet free-electron laser oscillator," *N. J. Phys.* **22**(7), 073058 (2020).
40. G. Paraskaki et al., "Optimization and stability of a high-gain harmonic generation seeded oscillator amplifier," *Phys. Rev. Accel. Beams* **24**, 34801 (2021).
41. H. Sun et al., "Seeding with a harmonic optical klystron resonator configuration in a high repetition rate free electron laser," *Phys. Rev. Accel. Beams* **25**, 060701 (2022).
42. D. Dunning, N. Thompson, and B. McNeil, "Design study of an HHG-seeded harmonic cascade free-electron laser," *J. Mod. Opt.* **58**(16), 1362–1373 (2011).
43. X. Wang et al., "High-repetition-rate seeded free-electron laser with direct-amplification of an external coherent laser," *N. J. Phys.* **24**(3), 33013 (2022).
44. Q. Jia, "Analysis of modulation parameters for high repetition rate seeded FEL," *Nucl. Instrum. Methods Phys. Res., Sect. A* **1015**, 165767 (2021).
45. L. H. Yu and J. Wu, "Theory of high gain harmonic generation: an analytical estimate," *Nucl. Instrum. Methods Phys. Res., Sect. A* **483**(1–2), 493–498 (2002).
46. Z. Huang and K. J. Kim, "Review of X-ray free-electron laser theory," *Phys. Rev. ST Accel. Beams* **10**(3), 034801 (2007).
47. Z. Huang et al., "Suppression of microbunching instability in the linac coherent light source," *Phys. Rev. ST Accel. Beams* **7**(7), 73–82 (2004).
48. S. Reiche, "Genesis 1.3: a fully 3D time-dependent FEL simulation code," *Nucl. Instrum. Methods Phys. Res., Sect. A* **429**(1), 243–248 (1999).
49. B. Liu et al., "The SXFEL upgrade: from test facility to user facility," *Appl. Sci.* **12**(1), 176 (2022).
50. C. Feng et al., "Coherent and ultrashort soft X-ray pulses from echo-enabled harmonic cascade free-electron lasers," *Optica* **9**, 785–791 (2022).
51. E. Saldin, E. Schneidmiller, and M. V. Yurkov, *The Physics of Free Electron Lasers*, Springer Science & Business Media (1999).
52. A. Marinelli et al., "HGHG schemes for short wavelengths," *Nucl. Instrum. Methods Phys. Res., Sect. A* **593**, 35–38 (2008).
53. P. Finetti et al., "Pulse duration of seeded free-electron lasers," *Phys. Rev. X* **7**, 021043 (2017).
54. G. Wang et al., "Beam energy distribution influences on density modulation efficiency in seeded free-electron lasers," *Phys. Rev. ST Accel. Beams* **18**, 060701 (2015).
55. C. Feng et al., "Measurement of the average local energy spread of electron beam via coherent harmonic generation," *Phys. Rev. ST Accel. Beams* **14**(9), 090701 (2011).
56. E. Allaria and G. De Ninno, "Soft-X-ray coherent radiation using a single-cascade free-electron laser," *Phys. Rev. Lett.* **99**, 014801 (2007).
57. B. Garcia et al., "Method to generate a pulse train of few-cycle coherent radiation," *Phys. Rev. Accel. Beams* **19**, 090701 (2016).
58. K. Zhou et al., "Generating high-brightness and coherent soft X-ray pulses in the water window with a seeded free-electron laser," *Phys. Rev. Accel. Beams* **20**(1), 010702 (2017).
59. G. Lambert et al., "Injection of harmonics generated in gas in a free-electron laser providing intense and coherent extreme-ultraviolet light," *Nat. Phys.* **4**, 296–300 (2008).
60. M. Labat et al., "High-gain harmonic-generation free-electron laser seeded by harmonics generated in gas," *Phys. Rev. Lett.* **107**, 224801 (2011).
61. S. Ackermann et al., "Generation of coherent 19- and 38-nm radiation at a free-electron laser directly seeded at 38 nm," *Phys. Rev. Lett.* **111**, 114801 (2013).

**Hanxiang Yang** received his BS degree from Lanzhou University in 2019. He is currently a PhD student under the supervision of Prof. Haixiao Deng at Shanghai Institute of Applied Physics, Chinese Academy of Sciences. Now, his research interests are focused on free-electron laser physics.

**Jiawei Yan** received his PhD in 2021 from Shanghai Institute of Applied Physics, Chinese Academy of Sciences under the supervision of Prof. Haixiao Deng. He is currently a physicist at the European XFEL. His research interests include free-electron laser physics, electron beam dynamics, and machine learning.

**Haixiao Deng** received his PhD from Shanghai Institute of Applied Physics, Chinese Academy of Sciences in 2009. He is currently a professor at Shanghai Advanced Research Institute, Chinese Academy of Sciences. His research interest focuses on particle accelerator-based light sources.